





Article

# Electrochemical Investigation of Iron-Catalyzed Atom Transfer Radical Polymerization

Gianluca Gazzola <sup>1,†</sup>, Sebastiano Pasinato <sup>1,†</sup>, Marco Fantin <sup>1</sup>, Niccolò Braidi <sup>2</sup> , Cristina Tubaro <sup>1</sup> , Christian Durante <sup>1</sup>  and Abdirisak Ahmed Isse <sup>1,\*</sup> 

<sup>1</sup> Department of Chemical Sciences, University of Padova, Via Marzolo 1, 35131 Padova, Italy

<sup>2</sup> Department of Chemical and Geological Sciences, University of Modena and Reggio Emilia, Via Campi 103, 41125 Modena, Italy

\* Correspondence: abdirisak.ahmedisse@unipd.it

† These authors contributed equally to this work.

**Abstract:** Use of iron-based catalysts in atom transfer radical polymerization (ATRP) is very interesting because of the abundance of the metal and its biocompatibility. Although the mechanism of action is not well understood yet, iron halide salts are usually used as catalysts, often in the presence of nitrogen or phosphorous ligands (L). In this study, electrochemically mediated ATRP (*e*ATRP) of methyl methacrylate (MMA) catalyzed by FeCl<sub>3</sub>, both in the absence and presence of additional ligands, was investigated in dimethylformamide. The electrochemical behavior of FeCl<sub>3</sub> and FeCl<sub>3</sub>/L was deeply investigated showing the speciation of Fe(III) and Fe(II) and the role played by added ligands. It is shown that amine ligands form stable iron complexes, whereas phosphines act as reducing agents. *e*ATRP of MMA catalyzed by FeCl<sub>3</sub> was investigated in different conditions. In particular, the effects of temperature, catalyst concentration, catalyst-to-initiator ratio, halide ion excess and added ligands were investigated. In general, polymerization was moderately fast but difficult to control. Surprisingly, the best results were obtained with FeCl<sub>3</sub> without any other ligand. Electrogenerated Fe(II) effectively activates the dormant chains but deactivation of the propagating radicals by Fe(III) species is less efficient, resulting in dispersity > 1.5, unless a high concentration of FeCl<sub>3</sub> is used.

**Keywords:** iron catalysts; *e*ATRP; methyl methacrylate; radical polymerization



**Citation:** Gazzola, G.; Pasinato, S.; Fantin, M.; Braidi, N.; Tubaro, C.; Durante, C.; Isse, A.A.

Electrochemical Investigation of Iron-Catalyzed Atom Transfer Radical Polymerization. *Molecules* **2022**, *27*, 6312. <https://doi.org/10.3390/molecules27196312>

Academic Editors: Haichao Xu, Mekki Bayachou and Lauro Tatsuo Kubota

Received: 27 August 2022

Accepted: 20 September 2022

Published: 24 September 2022

**Publisher's Note:** MDPI stays neutral with regard to jurisdictional claims in published maps and institutional affiliations.



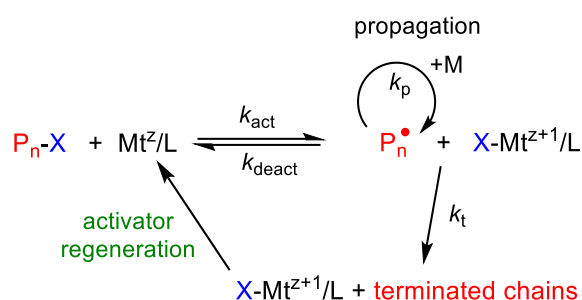
**Copyright:** © 2022 by the authors. Licensee MDPI, Basel, Switzerland. This article is an open access article distributed under the terms and conditions of the Creative Commons Attribution (CC BY) license (<https://creativecommons.org/licenses/by/4.0/>).

## 1. Introduction

Reversible deactivation radical polymerization (RDRP) techniques allow for the preparation of polymeric materials with precisely tailored architectures, low dispersity and well-preserved chain end functionality [1]. Among these methods, the most important and widely used techniques are atom transfer radical polymerization (ATRP [2–4]), reversible addition fragmentation chain transfer polymerization [5,6] and nitroxide-mediated polymerization [7,8]. The success of these methods relies on establishing a dynamic equilibrium between the propagating radical and a dormant species, which drastically reduces the rate of termination reactions, resulting in a remarkable increase in radical lifetime.

ATRP uses a transition metal complex, mainly Cu with a nitrogen-based ligand [3], to establish the equilibrium between a dormant polymer chain and the corresponding active radical. A metal complex at a low oxidation state ( $Mt^z/L$ ) reacts with an alkyl halide (RX) initiator or a halogen-capped dormant polymer chain ( $P_n-X$ ) to produce a propagating radical ( $P_n^\bullet$ ) and the metal complex at a higher oxidation state ( $X-Mt^{z+1}/L$ ) with the halide ion as an additional ligand (Scheme 1). This activation step occurs according to an inner-sphere electron transfer mechanism [9–11]. The radical propagates for a short period before it is quenched by the deactivator complex  $X-Mt^{z+1}/L$  to form a dormant species. The equilibrium constant,  $K_{ATRP} = k_{act}/k_{deact}$ , defines the equilibrium concentration of

propagating radicals and, hence, plays a crucial role in polymerization kinetics and control over molecular weight distribution.



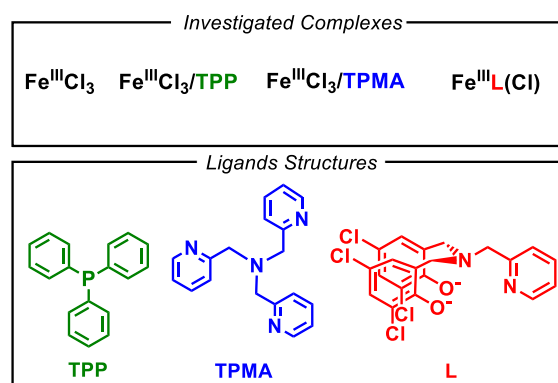
**Scheme 1.** General mechanism of ATRP with a reduction loop for activator regeneration (X = Cl, Br).

Several advanced variants of ATRP have been developed to reduce catalyst loading and improve the industrial attractiveness of the process. In these methods, the process starts with an oxygen-stable metal catalyst at a high oxidation state, while the activator catalyst—the metal at a lower oxidation state—is (re)generated in situ through various approaches [12]. Examples of these methods include activators regenerated by electron transfer (ARGET) ATRP [13–15] and supplemental activator and reducing agent (SARA) ATRP (also known as SET LRP) [16–18], which use a homogeneous reducing agent and a zero-valent metal, respectively, and methods based on external stimuli via electrochemistry [19,20], photochemistry [21–23] and sonochemistry [24,25]. Metal-free photo-induced ATRP is also widely used [26,27].

Although Cu is the most popular metal in ATRP, polymerizations have successfully been carried out with catalysts based on a large variety of other metals, such as Re, Fe, Ru, Os, Rh, Co, Ni and Pd [28]. Of these, iron has attracted considerable interest because it presents several advantages over copper catalysts. Indeed, iron is an extremely abundant metal in the Earth's crust and biocompatible iron-based systems can potentially be used for biomedical applications [29,30]. Therefore, iron can be considered a very promising metal in view of industrial development of ATRP. Like Cu and other metal catalysts, the activity of Fe-based catalysts strongly depends on the nature and structure of the ligands [31]. Most Fe catalysts used in ATRP are based on iron halide salts,  $\text{FeX}_3$  and/or  $\text{FeX}_2$ , in the absence or presence of added ligands, mainly based on nitrogen and phosphorous [32].

Both conventional ATRP based on Fe(II) [33–35] and advanced variants, such as initiators for continuous activator regeneration (ICAR) ATRP [36–39], ARGET ATRP [40,41], photo-induced ATRP [39,42,43] and electrochemically mediated ATRP (*e*ATRP) [44–46], have been used. Iron-based biocatalysts have also been successfully used in surface-initiated ATRP [47] as well as in solution phase [48,49], with interesting applications in biosensing [50–52]. *e*ATRP is particularly attractive because it is environmentally friendly, as no chemical reducing agents are used and it allows easy regulation of polymerization rate and accurate temporal control [53,54]. Unlike copper-catalyzed radical polymerization, for which *e*ATRP has been successfully applied to a wide range of monomers in various reaction media [19,20], *e*ATRP with Fe-based catalysts has rarely been investigated. The first application of electrochemistry to trigger controlled radical polymerization was reported by Amatore and co-workers who investigated the reaction of electrogenerated  $\text{Fe}^{\text{II}}(\text{salen})$  ( $\text{H}_2\text{salen} = N,N'$ -bis(salicylidene)ethylenediamine) with some alkyl halide initiators and its application to styrene polymerization [55]. More recently, Guo et al. [44,45] and Wang et al. [46] reported *e*ATRP of methyl methacrylate (MMA) catalyzed by iron halide salts, with or without tris(4-methoxyphenyl)-phosphine as an additional ligand, respectively.

Herein, we report a deeper investigation on the electrochemical behavior of the most common iron-based catalysts used in ATRP. The study also addresses the role of added ligands, such as chloride anions, amine-bis(phenolate), phosphines and amines (structures in Scheme 2), on *e*ATRP of MMA.



**Scheme 2.** Investigated Fe complexes. TPP = triphenylphosphine; TPMA = tris(2-pyridylmethyl)amine; L = 2-pyridylamino-*N,N*-bis(2-methylene-4,6-dichlorophenolate).

## 2. Results and Discussion

### 2.1. Cyclic Voltammetry of $\text{FeCl}_3$

Figure 1 shows cyclic voltammetry (CV) of  $\text{FeCl}_3$  in DMF + 0.1 M  $\text{Et}_4\text{NBF}_4$ , recorded at different scan rates. A well-defined cathodic peak (B) around  $-0.5$  V and a shoulder (A) around  $-0.2$  V are observed in the cathodic scan, while two anodic peaks, labelled  $A'$  and  $B'$ , are observed upon scan reversal. The voltammetric behavior of the iron salt strongly depends on scan rate ( $v$ ). The cathodic peak B and the shoulder shift to more negative potentials when  $v$  is increased while the normalized peak current of peak B,  $I_p(\text{B})/v^{1/2}$ , shows only a slight decrease. Conversely, major changes with  $v$  occur in the reverse scan. As  $v$  increases, peak  $A'$  increases at the expense of peak  $B'$ , which instead decreases. It is clear that more than one Fe(III) species is present in solution and, above all, the electrogenerated Fe(II) is distributed in different species with distinct oxidation potentials.

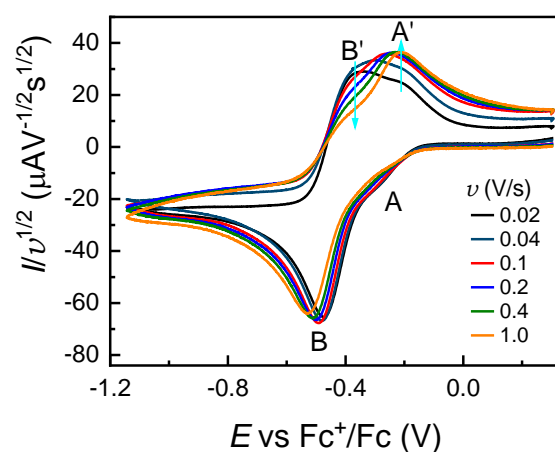


**Figure 1.** Cyclic voltammetry of 1 mM  $\text{FeCl}_3$  in DMF + 0.1 M  $\text{Et}_4\text{NBF}_4$  recorded on a GC electrode at different scan rates at  $T = 25$  °C.

The dependence of the relative intensities of peaks  $A'$  and  $B'$  on scan rate points out the existence of chemical reactions between the Fe(II) species involved in the oxidation processes at these peaks. Before making any hypothesis on the identity of these Fe(II) species, we attempted to identify the principal Fe(III) species present in solution. To this end, CV of a DMF solution of  $\text{FeCl}_3$  was investigated in the presence of added chloride ions. As shown in Figure 2, both the shoulder (A) and the anodic peak  $A'$  decreased and eventually disappeared as  $[\text{Cl}^-]$  was increased. When a large excess of  $\text{Cl}^-$  was added, a single peak couple ( $B/B'$ ) remained. This peak couple can be assigned to the  $\text{FeCl}_4^-/\text{FeCl}_4^{2-}$  redox couple. The separation between the anodic and cathodic peak potentials,  $\Delta E_p = E_{p,B'} - E_{p,B}$ , is 71 mV at  $v = 0.01$  V/s and increases with scan rate

(at  $v = 1 \text{ V/s}$ ,  $\Delta E_p = 118 \text{ mV}$ ). Therefore, the redox process under the peak couple is a quasi-reversible electron transfer. The half-wave potential calculated as the mid-point between the cathodic and anodic peaks,  $E_{1/2} = (E_{p,B'} + E_{p,B})/2$  does not depend on  $v$  and the average value measured at different scan rates is  $-0.499 \pm 0.003 \text{ V vs. Fc}^+/\text{Fc}$ .

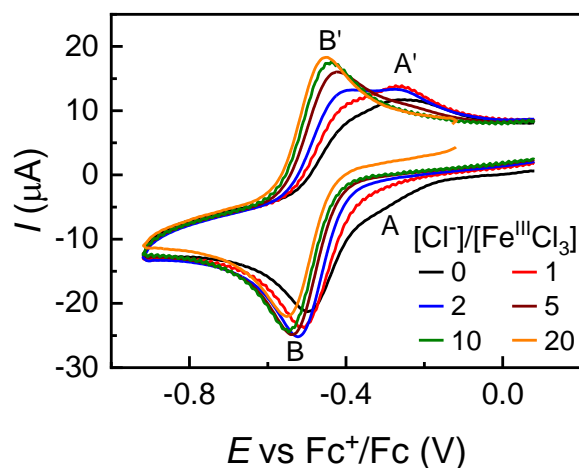


**Figure 2.** Cyclic voltammetry of 1 mM  $\text{FeCl}_3$  in DMF + 0.1 M  $\text{Et}_4\text{NBF}_4$  recorded on a GC electrode at  $v = 0.2 \text{ V/s}$  and  $T = 25 \text{ }^\circ\text{C}$ , before and after addition of different amounts of  $\text{Et}_4\text{NCl}$ .

When  $\text{FeCl}_3$  is dissolved in DMF, it undergoes speciation into  $\text{FeCl}_4^-$ ,  $\text{FeCl}_2^+$  and arguably some other Fe(III) species. Dass and George [56] investigated the speciation of iron(III)-chloro complexes in DMF by ultraviolet absorption spectroscopy. They concluded that dissolving  $\text{FeCl}_3$  in DMF produces mainly  $\text{FeCl}_4^-$  and  $\text{FeCl}_2^+$  together with small amounts of  $\text{FeCl}^{2+}$ . Kim and Park [57] investigated the structure of the adduct obtained by complexation of  $\text{FeCl}_3$  with DMF. They prepared the adduct by dissolving ferric chloride in DMF, followed by slow vacuum evaporation of excess DMF. After careful analysis of the solid with various techniques, they assigned the chemical formula  $[\text{Fe}^{\text{III}}\text{Cl}_2(\text{DMF})_{1.2}(\text{H}_2\text{O})_{2.7}]^+ [\text{Fe}^{\text{III}}\text{Cl}_4(\text{DMF})_{2.1}]^-$  to the adduct. Although the adduct was isolated only in the solid state, it likely arises from dichloro- and tetrachloro-iron(III) species in solution, which crystallize as an adduct when all excess solvent molecules are removed by evaporation. This study also confirmed that the preferred coordination number of iron(III) is 6. Throughout this paper, we will assume that all iron halide species are hexacoordinated, but for the sake of simplicity, we will omit coordinating solvent molecules.

Interestingly, CV of  $\text{FeCl}_2$  showed almost the same pattern previously observed for  $\text{FeCl}_3$ , except that the process now starts with the oxidation of Fe(II) to Fe(III) species. A broad anodic peak standing for two ill-resolved peaks is observed in the initial positive-going scan, while two well-defined peaks are observed in the reverse cathodic scan (Figure 3). When  $\text{FeCl}_2$  is dissolved in DMF, possibly the principal species present in solution is  $\text{FeCl}_2$  with minor formation of  $\text{FeCl}_4^{2-}$  so that the main anodic peak is  $A'$ . After oxidation, the electrogenerated iron(III) species will undergo a new speciation equilibrium with significant presence of both  $\text{FeCl}_4^-$  and  $\text{FeCl}_2^+$ . Reduction of this mixture in the reverse scan shows both peaks A and B. When increasing amounts of  $\text{Cl}^-$  were added, the B/B' peak couple progressively increased while A/A' decreased and disappeared in the presence of excess  $\text{Cl}^-$  (Figure 3). The peak couple obtained from  $\text{FeCl}_2$  with excess  $\text{Cl}^-$  had the same characteristics of that obtained from  $\text{FeCl}_3$  in the same conditions, indicating that the same redox couple is involved in both cases.

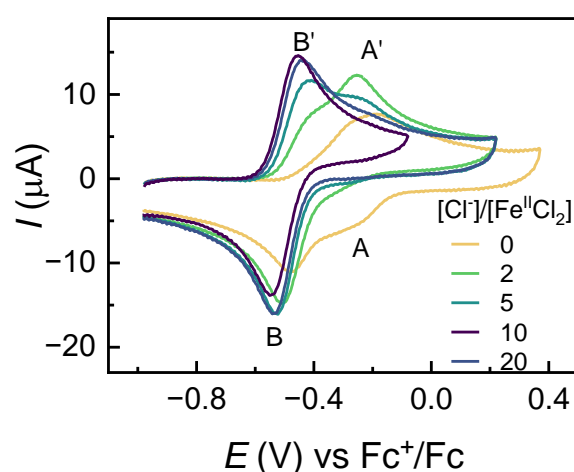


**Figure 3.** Cyclic voltammetry of 1 mM FeCl<sub>2</sub> in DMF + 0.1 M Et<sub>4</sub>NBF<sub>4</sub> recorded on a GC electrode at  $v = 0.2$  V/s and  $T = 25$  °C, before and after addition of different amounts of Et<sub>4</sub>NCl.

The set of analyses so far discussed allows for unambiguous assignment of peak couple B/B' to FeCl<sub>4</sub><sup>2-</sup>/FeCl<sub>2</sub><sup>2-</sup>. Considering the well-documented presence of FeCl<sub>2</sub><sup>+</sup> in DMF solutions of FeCl<sub>3</sub> and the voltametric pattern of FeCl<sub>2</sub>, we assign peaks A/A' to the FeCl<sub>2</sub><sup>-</sup>/FeCl<sub>2</sub> redox couple.



Let us now discuss the unusual scan-rate dependence of peaks A' and B' in Figure 1. The B/B' peak couple is partially reversible at low scan rates, which can be taken to be indicative of partial disappearance of FeCl<sub>4</sub><sup>2-</sup> during the scan. One would then expect to see more reversibility when the scan rate is increased and, hence, the overall electrode reaction time is reduced. Surprisingly, the opposite scenario is observed: the peak couple tends toward full irreversibility at higher scan rates, while peak A' increases (Figure 1). To rationalize this behavior, we have to consider a fast equilibrium between two iron(II) species:



If this equilibrium is fast and well shifted to the right, FeCl<sub>4</sub><sup>2-</sup> will be converted to FeCl<sub>2</sub> as soon as it is generated by electroreduction of FeCl<sub>4</sub><sup>2-</sup> at peak B. At high scan rates, the voltametric pattern will be more akin to the equilibrium situation: small equilibrium FeCl<sub>4</sub><sup>2-</sup> concentration, small or hardly perceptible anodic peak B'. At low scan rates, the overall oxidation process at peak B' continues occurring for a much longer time. When the small quantity of FeCl<sub>4</sub><sup>2-</sup> initially present at equilibrium is consumed, reaction (3) is shifted to the left to restore the equilibrium, but FeCl<sub>4</sub><sup>2-</sup> continues to be oxidized, producing, at the end, a signal much higher than predicted according to the equilibrium concentration of FeCl<sub>4</sub><sup>2-</sup>. In other words, the anodic peak B' arises from a sequence of two reactions, as shown in Equation (4). Indeed, this sequence is at play also at high scan rates, but its effect is negligible because the scan rate is so high that the experiment ends before FeCl<sub>4</sub><sup>2-</sup> is regenerated to any appreciable extent by reaction (3). Iron(II) is present in solution either as FeCl<sub>4</sub><sup>2-</sup> or FeCl<sub>2</sub>. At low scan rates, the kinetics of equilibrium (3) affects the overall oxidation process and peak B' becomes more prominent than peak A'. Conversely, when at high scan rates, the effect of the backward reaction in Equation (3) becomes negligible, the oxidation process is more representative of the equilibrium conditions and A' becomes the only observable anodic peak.



Starting from either FeCl<sub>3</sub> or FeCl<sub>2</sub>, it is possible to prepare DMF solutions containing exclusively FeCl<sub>4</sub><sup>−</sup> or FeCl<sub>4</sub><sup>2−</sup> and determine the redox properties of FeCl<sub>4</sub><sup>−</sup>/FeCl<sub>4</sub><sup>2−</sup>. Independent experiments on FeCl<sub>3</sub> and FeCl<sub>2</sub> performed in DMF + 0.1 M Et<sub>4</sub>NBF<sub>4</sub> in the presence of a large excess of Cl<sup>−</sup> gave  $E_{1/2} = -0.499 \pm 0.003$  V vs. Fc<sup>+</sup>/Fc and diffusion coefficients,  $D$ , of  $(8.0 \pm 0.8) \times 10^{-6}$  cm<sup>2</sup> s<sup>−1</sup> and  $(2.3 \pm 0.1) \times 10^{-6}$  cm<sup>2</sup> s<sup>−1</sup> for FeCl<sub>4</sub><sup>−</sup> and FeCl<sub>4</sub><sup>2−</sup>, respectively (Figures S1 and S2). The diffusion coefficients were calculated from cyclic voltammetry according to the equation of Randles–Sevcik [58]. These data can be used to determine the standard potential of the redox couple according to Equation (5):

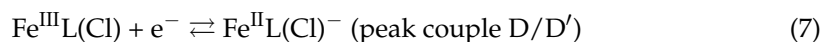
$$E_{1/2} = E^{\circ'} + \frac{RT}{F} \ln \left( \frac{D_{\text{Red}}}{D_{\text{Ox}}} \right)^{1/2} \quad (5)$$

where  $E^{\circ'}$  is the formal potential,  $R$  is the universal gas constant,  $F$  is the Faraday constant and Ox and Red stand for the oxidized and reduced forms of the redox couple. Approximately assuming  $E^{\circ} = E^{\circ'}$  gave  $E^{\circ} = -0.483 \pm 0.003$  V vs. Fc<sup>+</sup>/Fc. The standard electron transfer rate constant,  $k^{\circ}$ , was determined by the method of Nicholson [59]. Assuming a value of 0.5 for the transfer coefficient,  $\alpha$ ,  $\Delta E_p$  values obtained from CVs of both FeCl<sub>4</sub><sup>−</sup> and FeCl<sub>4</sub><sup>2−</sup> were fit to the theoretical working curve of Nicholson (Figure S3). Both data series showed excellent fits and produced an average  $k^{\circ}$  value of  $(1.21 \pm 0.36) \times 10^{-2}$  cm s<sup>−1</sup>.

## 2.2. Cyclic Voltammetry of

### *Chloro(2-pyridylamino-N,N-bis(2-methylene-4,6-dichlorophenolate))iron(III), Fe<sup>III</sup>L(Cl)*

The amine-bis(phenolate) complex Fe<sup>III</sup>L(Cl) in solution likely exhibits a trigonal bipyramidal five-coordinate geometry, with four coordination sites occupied by L and one by the chlorine anion or by a solvent molecule [60]. Cyclic voltammetry of Fe<sup>III</sup>L(Cl) shows two cathodic peaks labeled C and D and only one anodic peak (labeled C') in the reverse scan (Figure 4). This pattern did not change when the scan rate was increased. When instead excess Cl<sup>−</sup> was added to the solution, peaks C and C' disappeared while a new anodic peak (labeled D') appeared. The voltametric behavior of Fe<sup>III</sup>L(Cl) can be rationalized by considering the presence of a small amount of Fe<sup>III</sup>L<sup>+</sup> together with Fe<sup>III</sup>L(Cl), which is the principal Fe(III) species present in solution. When Cl<sup>−</sup> is added in large excess over Fe(III), Fe<sup>III</sup>L<sup>+</sup> is converted to Fe<sup>III</sup>L(Cl). Therefore, peaks C and D can be attributed to the reduction of Fe<sup>III</sup>L<sup>+</sup> and Fe<sup>III</sup>L(Cl), respectively. The assignment of the anodic peaks D' and C' is also straightforward. They are coupled with the cathodic peaks C and D, respectively. Thus, the observed voltametric pattern stands for the following one-electron redox reactions:



Fe<sup>III</sup>L<sup>+</sup> arises from partial dissociation of Fe<sup>III</sup>L(Cl) in DMF, but a small amount of Cl<sup>−</sup> is enough to convert all Fe<sup>III</sup>L<sup>+</sup> in solution into Fe<sup>III</sup>L(Cl). Indeed, peak C almost disappears as soon as the [Cl<sup>−</sup>] / [Fe<sup>III</sup>L(Cl)] reaches 0.5. Notably, however, the appearance of peak D' and its development to a full peak, as well as the disappearance of peak C', require addition of a large excess of Cl<sup>−</sup> over Fe<sup>III</sup>L(Cl). Fe<sup>II</sup>L(Cl)<sup>−</sup> generated in reaction (7) rapidly and reversibly dissociates to Fe<sup>II</sup>L and Cl<sup>−</sup> (Equation (8)). Thus, when low [Cl<sup>−</sup>] / [Fe<sup>III</sup>L(Cl)] is used, the oxidation peak of Fe<sup>II</sup>L remains well evident, even if there is no Fe<sup>III</sup>L<sup>+</sup> in solution (peak C is absent). A large excess of Cl<sup>−</sup> is required to fully suppress the dissociation reaction and set the conditions for one-electron reduction of Fe<sup>III</sup>L(Cl) without complications due to a chemical reaction following the electron transfer.



The redox properties of Fe<sup>III</sup>L(Cl) were further investigated to determine  $E^{\circ}$  and  $k^{\circ}$  in DMF in the presence of Cl<sup>−</sup> with [Cl<sup>−</sup>] / [Fe<sup>III</sup>L(Cl)] = 30. A quasi-reversible peak couple



with scan rate-dependent  $\Delta E_p$  was observed (Figure S4). The half-wave potential calculated as the average of the values measured at different scan rates is  $-0.853 \pm 0.001$  V vs.  $\text{Fc}^+/\text{Fc}$ . Assuming similar diffusion coefficients for  $\text{Fe}^{\text{III}}\text{L}(\text{Cl})$  and  $\text{Fe}^{\text{II}}\text{L}(\text{Cl})^-$  and neglecting the activity coefficient contribution in Equation (5), the measured  $E_{1/2}$  can be approximately taken as  $E^\circ$ . The standard heterogeneous rate constant of electron transfer was determined by the method of Nicholson [59], assuming  $\alpha = 0.5$ . The best fit of the experimental data on the working curve (Figure S5) gave  $k^\circ = (1.10 \pm 0.04) \times 10^{-3} \text{ cm s}^{-1}$ .

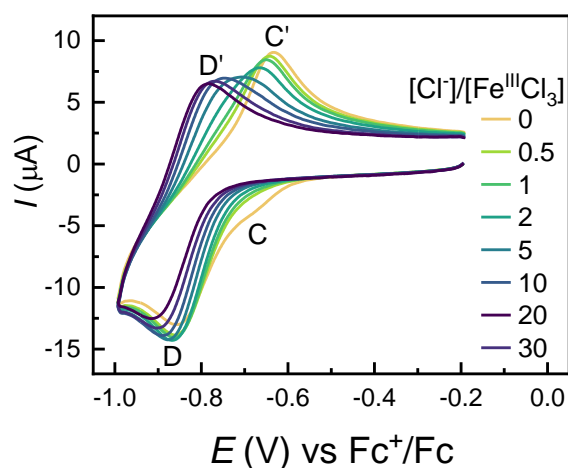


**Figure 4.** Cyclic voltammetry of 1 mM  $\text{Fe}^{\text{III}}\text{L}(\text{Cl})$  in DMF + 0.1 M  $\text{Et}_4\text{NBF}_4$  recorded on a GC electrode at  $v = 0.2$  V/s and  $T = 25$  °C, before and after addition of different amounts of  $\text{Et}_4\text{NCl}$ .

### 2.3. Cyclic Voltammetry of $\text{FeCl}_3$ in the Presence of Other Ligands

Phosphorous- and nitrogen-based ligands are often used as additional ligands in  $\text{FeX}_3$ -catalyzed ATRP.  $\text{FeX}_3$  is often mixed with a ligand L with the assumption that a more active catalyst species  $\text{FeX}_3/\text{L}$  is formed. We investigated the role of triphenylphosphine (TPP) and tris(2-pyridylmethyl)amine (TPMA), taken as examples of phosphorous and nitrogen ligands, respectively, on the redox behavior of  $\text{FeCl}_3$ .

Figure 5a shows CVs recorded for  $\text{FeCl}_3$  before and after addition of TPP. No change in the voltametric pattern of the iron chloride complex(es) was observed. A similar result was obtained by UV-vis analysis. The absorption spectrum recorded after addition of TPP was simply the superimposition of the separate spectra of  $\text{FeCl}_3$  and TPP (Figure S6). The voltametric pattern of  $\text{FeCl}_2$  was also unaffected by TPP (Figure S7). These results clearly show that TPP does not form new complexes with  $\text{FeCl}_3$  or  $\text{FeCl}_2$  in the investigated reaction conditions. Walker and Poli [61] reported the synthesis of  $\text{FeCl}_3$ -phosphine complexes of general formula  $\text{FeCl}_3(\text{PR}_3)_2$  ( $\text{R} = \text{Me}, \text{Ph}, \text{cyclohexyl}$ ). The compounds were prepared at low temperature in nonpolar solvents, such as benzene and toluene, but their solutions were unstable at room temperature or higher. Phosphine complexes of  $\text{FeX}_2$  were reported by Sawamoto and co-workers as  $\text{FeX}_2(\text{L}_2)$  ( $\text{X} = \text{Cl}, \text{L} = \text{PMePh}_2$ ;  $\text{X} = \text{Br}, \text{L} = \text{PMePh}_2, \text{PPh}_3, \text{P}(n\text{-Bu})_3$ ) [34]. They were prepared in toluene and used as ATRP catalysts in the same solvent at 80 °C. Although these complexes seem to be stable in these reaction conditions, their stability and chemical structure in polar solvents, such as DMF, are yet to be proved.

To check whether TPP can reduce  $\text{Fe}(\text{III})$  to  $\text{Fe}(\text{II})$ , a mixture of  $\text{FeCl}_3$  with a two-fold excess of TPP in DMF + 0.1 M  $\text{Et}_4\text{NBF}_4$  was monitored by linear sweep voltammetry (LSV) at a rotating disc electrode at room temperature. LSV recorded at  $t = 0$  was identical with that observed before TPP addition and showed a well-defined wave for the reduction of  $\text{Fe}(\text{III})$  to  $\text{Fe}(\text{II})$  with a cathodic limiting current,  $|I_{L,c}| = 56 \mu\text{A}$ . Since the system initially contained only  $\text{Fe}(\text{III})$ , the anodic limiting current,  $I_{L,a}$ , was zero. The LSV recorded after 1 h showed a slight decrease in  $|I_{L,c}|$  together with small  $I_{L,a}$ . The reaction was left overnight and after 20 h, a significantly decreased  $\text{Fe}(\text{III})$  concentration accompanied by the build-up of  $\text{Fe}(\text{II})$  was observed, clearly indicating that  $\text{FeCl}_3$  was slowly reduced by TPP. The ability

of triphenylphosphines to act as reducing agents in iron-catalyzed ATRP has previously been suggested and, in a few cases, experimentally demonstrated [62,63]. The reaction between  $\text{FeCl}_3$  and TPP is very slow at room temperature and probably will not affect the rate of polymerization in such conditions. However, many Fe-catalyzed polymerizations, especially in the case of *m*MMA and styrene, are typically carried out at temperatures as high as 110 °C, where Fe(III) reduction by phosphines might be fast.

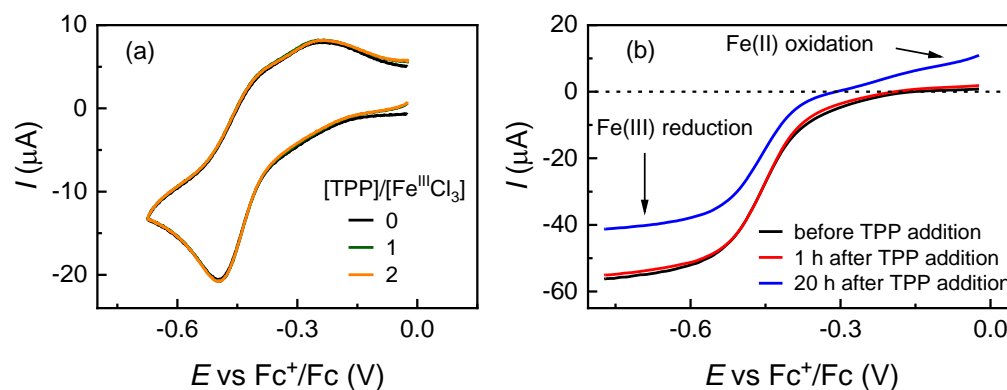
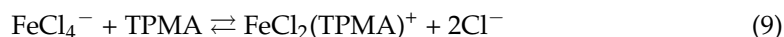


**Figure 5.** Voltammetry of 1.16 mM  $\text{FeCl}_3$  in DMF + 0.1 M  $\text{Et}_4\text{NBF}_4$  recorded on a GC electrode at  $T = 25\text{ }^\circ\text{C}$ ; (a) CV recorded at  $v = 0.2\text{ V/s}$  before and after addition of TPP; (b) linear sweep voltammometry on a rotating disc electrode at  $\omega = 2000\text{ rpm}$  and  $v = 0.005\text{ V/s}$ , recorded before and after addition of a 2-fold excess of TPP.

In contrast to TPP, the nitrogen ligand TPMA reacted rapidly and quantitatively with  $\text{FeCl}_3$ . Addition of 1 equiv. of TPMA to a solution of  $\text{FeCl}_3$  caused full disappearance of the original signal, which was replaced by a reversible peak couple at a less negative potential (Figure 6). Further addition of TPMA did not affect the voltammetric response. It is obvious that a new complex, in which both Fe(III) and Fe(II) are stable, is formed. TPMA complexes of both Fe(III) and Fe(II) are known in the literature [64,65]. They have a distorted octahedral geometry arising from tetra-coordination by TPMA plus coordination of chloride ions,  $\text{FeCl}_2(\text{TPMA})^+$  and  $\text{FeCl}_2(\text{TPMA})$ . Therefore, reactions (9) and (10) occur when TPMA is added to a DMF solution of  $\text{FeCl}_3$ . The standard reduction potential of  $\text{FeCl}_2(\text{TPMA})^+$  (Equation (11)) can be estimated as  $E^\circ \approx E_{1/2} = (E_{\text{pa}} + E_{\text{pc}})/2$ , where  $E_{\text{pa}}$  and  $E_{\text{pc}}$  are the anodic and cathodic peak potentials and the measured value is  $E_{1/2} = -0.211\text{ V vs. Fc}^+/\text{Fc}$ .



We examined the effect of  $\text{Cl}^-$  excess on the stability of  $\text{FeCl}_2(\text{TPMA})^+$ . Addition of a two-fold excess of  $\text{Cl}^-$  over  $\text{FeCl}_3$  did not affect the CV pattern of the iron-TPMA complex (Figure S8). A decrease in the cathodic peak of  $\text{FeCl}_2(\text{TPMA})^+$  together with the appearance of the cathodic peak of  $\text{FeCl}_4^-$  was observed only when a large excess of  $\text{Cl}^-$  was added. This indicates that Fe(III) has a much higher affinity for TPMA than  $\text{Cl}^-$ , but reaction (9) shifts to the left as the concentration of added  $\text{Cl}^-$  is increased. Notably, when in the presence of excess  $\text{Cl}^-$ , the principal iron species present in solution became  $\text{FeCl}_4^-$ , a reversible peak couple for the  $\text{FeCl}_4^- / \text{FeCl}_4^{2-}$  couple was not observed (Figure S8). This means that the stability constant of  $\text{FeCl}_2(\text{TPMA})$  is higher than that of  $\text{FeCl}_2(\text{TPMA})^+$ . Once  $\text{FeCl}_4^-$  is reduced to  $\text{FeCl}_4^{2-}$ , the latter rapidly reacts with TPMA to form  $\text{FeCl}_2(\text{TPMA})$ , so that the oxidation peak of  $\text{FeCl}_4^{2-}$  is missing while the anodic peak due to  $\text{FeCl}_2(\text{TPMA})$  oxidation is always present (Figure S8).



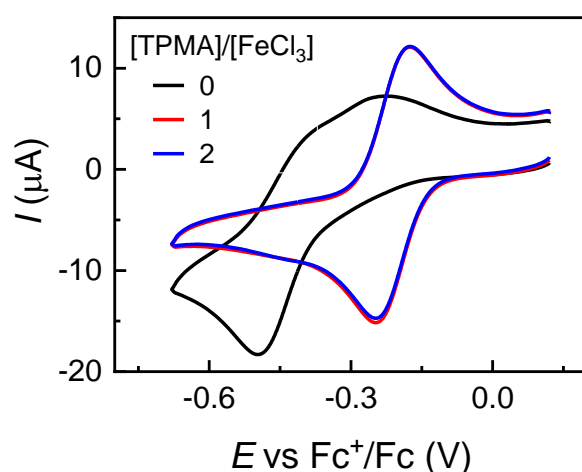


**Figure 6.** Cyclic voltammetry of 1.1 mM FeCl<sub>3</sub> in DMF + 0.1 M Et<sub>4</sub>NBF<sub>4</sub> recorded on a GC electrode at  $v = 0.2$  V/s and  $T = 25$  °C, before and after addition of TPMA.

In summary, the Fe(III) species formed in solution and their standard reduction potentials are summarized in Table 1. When no ligand is added or TPP is used as a ligand, the principal Fe(III) complex in solution is FeCl<sub>4</sub><sup>−</sup> with a characteristic  $E^\circ$  of  $-0.483$  V vs. Fc<sup>+</sup>/Fc. 2-pyridylamino-*N,N*-bis(2-methylene-4,6-dichlorophenolate) (L) forms a stable complex, Fe<sup>III</sup>L(Cl), with a cathodic shift of  $E^\circ$  of Fe(III)/Fe(II) by 0.37 V. TPMA also forms a stable complex with the iron salt, but the standard potential of the Fe(III)/Fe(II) couple shifts anodically by 0.272 V. In ATRP, a metal at a low oxidation state (Fe(II) in this case) reacts with an alkyl halide initiator, RX or a halogen-capped dormant species, P<sub>n</sub>-X, to generate the active radical species. The rate of this activation reaction is strongly dependent on  $E^\circ$  of the metal complex. Therefore, the expected order of activity of the Fe complexes examined here is Fe<sup>III</sup>L(Cl) > Fe<sup>III</sup>Cl<sub>4</sub><sup>−</sup> > Fe<sup>III</sup>Cl<sub>2</sub>(TPMA)<sup>+</sup>. However, in addition to the ability to activate RX, an efficient ATRP catalyst must also be a good radical deactivator; hence, predicting the overall efficacy of an iron catalyst, on the basis of  $E^\circ$  alone, is not straightforward.

**Table 1.** Standard reduction potentials of Fe(III) complexes in DMF + 0.1 M Et<sub>4</sub>NBF<sub>4</sub> at  $T = 25$  °C.

| Ligand         | Complex                               | $E^\circ$ vs. Fc <sup>+</sup> /Fc (V) |
|----------------|---------------------------------------|---------------------------------------|
| -              | FeCl <sub>4</sub> <sup>−</sup>        | −0.483                                |
| L <sup>1</sup> | FeL(Cl)                               | −0.853                                |
| TPP            | FeCl <sub>4</sub> <sup>−</sup>        | −0.483                                |
| TPMA           | FeCl <sub>2</sub> (TPMA) <sup>+</sup> | −0.211                                |

<sup>1</sup> L = 2-pyridylamino-*N,N*-bis(2-methylene-4,6-dichlorophenolate).

## 2.4. Electrochemically Mediated ATRP (eATRP)

### 2.4.1. eATRP Mediated by Amine-bis(phenolate) iron(III) Chloride, Fe<sup>III</sup>L(Cl)

The voltametric behavior of Fe<sup>III</sup>L(Cl) in 50 vol% mMA in DMF + 0.1 M Et<sub>4</sub>NBF<sub>4</sub> is slightly different from that in pure DMF. The pre-peak C is absent, whereas peak D shows partial reversibility (Figure S9). It appears that dissociation of Fe<sup>III</sup>L(Cl) to give Fe<sup>III</sup>L<sup>+</sup> and Cl<sup>−</sup> is disfavored in the monomer/solvent mixture. Further, Fe<sup>II</sup>L(Cl)<sup>−</sup> is more stable in mMA/DMF than in pure DMF. These changes are likely due to modifications of medium polarity, which decreases when mMA with a dielectric constant,  $\epsilon$ , of 6.53 at 25 °C [66] is added to DMF ( $\epsilon = 38.25$  at 20 °C [67]). The mixture has lower ability to solvate ions than pure DMF and, therefore, dissociation of Fe<sup>III</sup>L(Cl) and Fe<sup>II</sup>L(Cl)<sup>−</sup> becomes less favored in the mixture.

eATRP of mMA mediated by Fe<sup>III</sup>L(Cl) was carried out in 50/50 (V/V) DMF/MMA mixtures with 5 mM catalyst and 15 mM initiator. As initiators, ethyl  $\alpha$ -chlorophenyl acetate, ECPA, and ethyl  $\alpha$ -bromophenyl acetate, EBPA, which are among the most active alkyl

halides used in ATRP, were chosen. Nonetheless, CV tests revealed that electrogenerated  $\text{Fe}^{\text{II}}\text{L}(\text{Cl})^-$  reacts very slowly with these initiators (Figure S9). Since it was not easy to estimate  $E_{1/2}$  of the catalyst in the typical reaction conditions, the applied potential,  $E_{\text{app}}$ , was chosen with reference to the cathodic peak potential of the mediator (peak D). The reaction time was set at 4 h, but in some cases, polymerization was stopped earlier (2–3 h) because of drastic increase in viscosity.

The results of the electrochemically mediated polymerizations are collected in Table 2, whereas examples of reaction kinetics and trends of  $M_n$  and dispersity are shown in Figure 7. Using ECPA at 70 °C and  $E_{\text{app}} = E_p$ , 42.3% conversion was achieved after 4 h, but the reaction was not controlled. The dispersity of the polymer was very high and its molecular weight exceeded the theoretical value by about one order of magnitude (Table 2, entry 1). This first experiment indicated that activation was effective, but deactivation was inefficient. The experiment was then repeated with a 10-fold excess of  $\text{Cl}^-$  with respect to the iron mediator to increase the concentration of the deactivator  $\text{Fe}^{\text{III}}\text{L}(\text{Cl})$ . Again, the reaction was fast without any control (entry 2). Last, the temperature was lowered to 50 °C. The reaction was slower, but the dispersity remained very high and  $M_n$  was 20-fold higher than the theoretical value (entry 3). Two more experiments were performed with this mediator by changing the initiator to EBPA. Activation of this initiator by ATRP mechanism will produce  $\text{Fe}^{\text{III}}\text{L}(\text{Br})$ , which might be a better deactivator than  $\text{Fe}^{\text{III}}\text{L}(\text{Cl})$ . Disappointingly, the results were very similar to those obtained with ECPA (Table 2, entries 3–4 and Figure 7).

**Table 2.** *e*ATRP of methyl methacrylate (MMA) in DMF/monomer (50/50, V/V) + 0.1 M  $\text{Et}_4\text{NBF}_4$  <sup>1</sup>.

| Entry          | Initiator | $E_{\text{app}} - E_{\text{pc}}$<br>(V) | $T$<br>(°C) | $t$<br>(h) | $Q/Q_{\text{th}}$ <sup>2</sup> | Conv. <sup>3</sup><br>(%) | $10^3 k_{\text{app}}$ <sup>4</sup><br>( $\text{min}^{-1}$ ) | $M_{n,\text{GPC}}$ <sup>5</sup><br>(kDa) | $M_{n,\text{th}}$ <sup>6</sup><br>(kDa) | $\bar{D}$ <sup>5</sup> |
|----------------|-----------|---|-------------|------------|--------------------------------|---------------------------|---|--|---|------------------------|
| 1              | ECPA      | 0                                       | 70          | 4          | 0.81                           | 42.3                      | 2.35  | 147.80                                   | 13.26                                   | 2.75                   |
| 2 <sup>7</sup> | ECPA      | 0                                       | 70          | 3          | 0.75                           | 55.5                      | 3.27  | 157.06                                   | 17.34                                   | 2.18                   |
| 3              | ECPA      | 0                                       | 50          | 4          | 0.70                           | 17.6                      | 0.36  | 109.04                                   | 5.64                                    | 2.54                   |
| 4              | EBPA      | 0.06                                    | 50          | 2          | 0.93                           | 38.5                      | 4.40  | 94.67                                    | 12.38                                   | 2.34                   |
| 5              | EBPA      | −0.06                                   | 70          | 2          | 0.59                           | 40.0                      | 4.63  | 85.52                                    | 13.04                                   | 2.52                   |

<sup>1</sup>  $[\text{MMA}]:[\text{RX}]:[\text{Fe}^{\text{III}}\text{L}(\text{Cl})] = 100:0.32:0.11$ ;  $[\text{Fe}^{\text{III}}\text{L}(\text{Cl})] = 5$  mM, WE = Pt mesh, CE = graphite rod,  $V = 10$  mL.

<sup>2</sup> Ratio between passed charge and theoretical value calculated for  $1e^-$  reduction of  $\text{Fe}(\text{III})$ . <sup>3</sup> Monomer conversion.

<sup>4</sup> Apparent polymerization rate constant determined as the slope of  $\ln([\text{M}]_0/[\text{M}])$  vs.  $t$ . <sup>5</sup> Determined by GPC.

<sup>6</sup> Theoretical molecular weight. <sup>7</sup> In the presence of 0.05 M  $\text{Et}_4\text{NCl}$ .

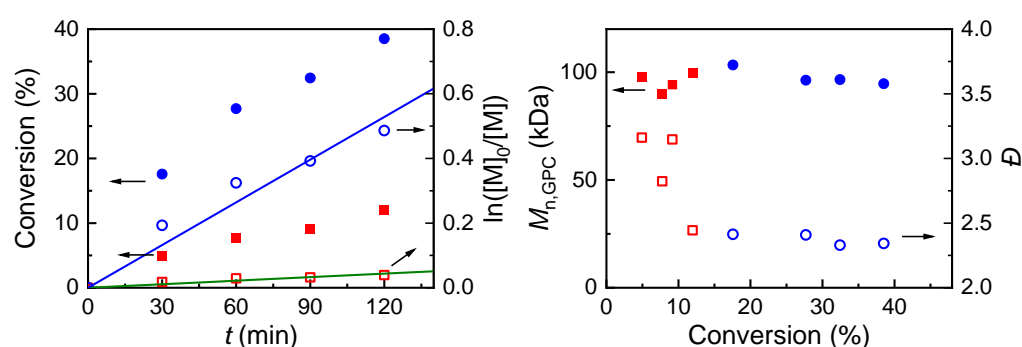


**Figure 7.** *e*ATRP of mMA mediated by  $\text{Fe}^{\text{III}}\text{L}(\text{Cl})$  in DMF/MMA (50/50, V/V) + 0.1 M  $\text{Et}_4\text{NBF}_4$  at  $T = 50$  °C, with ECPA as initiator (squares) at  $E_{\text{app}} = E_p$  or EBPA as initiator (circles) at  $E_{\text{app}} = E_p + 0.06$  V. Other conditions:  $[\text{MMA}]:[\text{RX}]:[\text{Fe}^{\text{III}}\text{L}(\text{Cl})] = 100:0.32:0.11$  with  $[\text{Fe}^{\text{III}}\text{L}(\text{Cl})] = 5$  mM.

Overall, the amine–bis(phenolate) iron(III) complex proved to be inefficient as a mediator of controlled radical polymerization of mMA in DMF under electrochemical generation of  $\text{Fe}(\text{II})$  activator species. This result is at variance with previous reports by Shaver and co-workers on well-controlled polymerizations of mMA and styrene mediated by various amine–bis(phenolate) iron(III) complexes in the presence of radical initiators, such as azobis(isobutyronitrile) [37,68]. There are, however, important differences between

the experimental conditions. All previous polymerizations were performed in bulk or in mixtures of monomer with nonpolar solvents. Further, the typical concentration of the iron(III) complex was nearly 100 mM. Last, the reactions were carried out at temperatures as high as 120 °C. Obviously these conditions are not desirable, especially the use of high catalyst concentration, which inevitably will involve costly polymer purification steps. *e*ATRP with this type of mediator was here investigated to explore the possibility of employing a low-catalyst load under mild conditions. The failure of control in low-catalyst-load *e*ATRP can be attributed to lack of deactivation. Schroeder and Buback [69] measured deactivation rate constants,  $k_{\text{deact}}$ , in iron-mediated ATRP. For an amine-bis(phenolate) iron(III) complex, they measured at 60 °C a  $k_{\text{deact}}$  value of about  $10^4 \text{ M}^{-1} \text{ s}^{-1}$ , which is 2 orders of magnitude lower than  $k_{\text{deact}}$  of copper complexes. This value increases by one order of magnitude if the temperature is raised to 120 °C. While deactivation rate in bulk monomer at 120 °C with high catalyst load is high enough to ensure control over molecular weight distribution, it is inefficient in *e*ATRP. Indeed, due to lower  $T$  and lower catalyst loading, it can be estimated that deactivation rate in the *e*ATRP experiments is at least 2 orders of magnitude lower than in the reaction conditions employed by Shaver and co-workers.

#### 2.4.2. *e*ATRP Mediated by $\text{FeCl}_3$

*e*ATRP of *m*MA mediated by iron halide complexes, both in the absence and presence of a phosphorous ligand, has already been reported [44–46]. These studies used  $\text{FeBr}_3$  and  $\text{FeCl}_3 \cdot 6\text{H}_2\text{O}$  with tris(2,4,6-methoxyphenyl)phosphine as an additional ligand or  $\text{FeCl}_3 \cdot 6\text{H}_2\text{O}$  without added ligand and, in most cases, the best results were obtained when quite high concentrations of iron salt were used. For comparison with  $\text{FeBr}_3$  and  $\text{FeCl}_3 \cdot 6\text{H}_2\text{O}$ , which was the principal catalyst in their study, Wang et al. [46] reported a single *e*ATRP experiment with  $\text{FeCl}_3$  [46]. Using ca 31 mM  $\text{FeCl}_3$  in *N*-methylpyrrolidone at 95 °C, they achieved 43% monomer conversion after ca 6.5 h, obtaining a polymer with dispersity  $D = 1.34$ .

Based on these previous studies, a relatively high concentration of  $\text{FeCl}_3$  was first considered. Before *e*ATRP experiments, the effect of  $[\text{FeCl}_3]$  and monomer on the voltametric behavior of Fe(III) was examined in conditions of *e*ATRP. Addition of *m*MA to DMF did not change the general CV pattern of  $\text{FeCl}_3$ , but peak A' became more pronounced while peak B gained more reversibility. The equilibrium distributions of both Fe(III) and Fe(II) species are influenced by medium polarity as well as initial  $\text{FeCl}_3$  concentration and temperature. The effect of  $[\text{FeCl}_3]$  is evidenced in Figure 8, which shows a remarkable enhancement of peak B' as  $[\text{FeCl}_3]$  is increased. In DMF/*m*MA, it is possible to estimate  $E_{1/2}$  of the  $\text{FeCl}_4^- / \text{FeCl}_4^{2-}$  redox couple as  $(E_{p,B} + E_{p,B'})/2$ , especially at high  $[\text{FeCl}_3]$  and low scan rates. The estimated value was  $-0.49 \text{ V}$  vs.  $\text{Fc}^+/\text{Fc}$ .

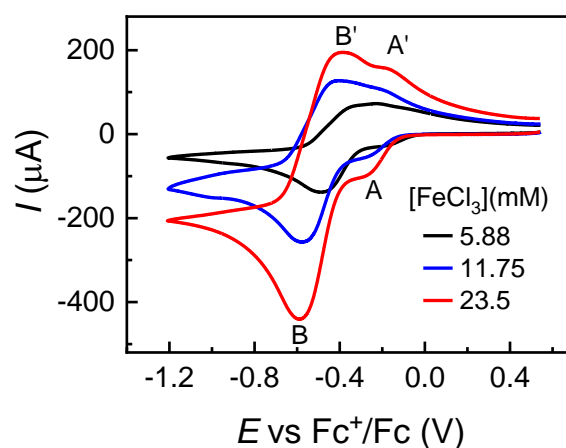


**Figure 8.** Cyclic voltammetry of  $\text{FeCl}_3$  in DMF/*m*MA (50/50, V/V) + 0.1 M  $\text{Et}_4\text{NBF}_4$  recorded on a GC electrode at  $v = 0.2 \text{ V/s}$  and  $T = 55 \text{ °C}$ .

The results of *e*ATRPs for *m*MMA performed at different conditions are summarized in Table 3. The applied potential,  $E_{app}$ , is reported as  $E_{app} - E_{1/2}$ , with reference to the value of  $E_{1/2}$  measured from CV before electrolysis. A first set of *e*ATRPs at 70 °C was carried out with 23.5 mM  $FeCl_3$  at different  $E_{app}$  values. All polymerizations were well controlled, obeying first-order kinetic rate laws and producing polymers with narrow molecular weight distribution, though the experimental molecular weights did not perfectly match the theoretical values (Figure 9).  $M_{n,GPC}$  was always greater than  $M_{n,th}$ , indicating initiation efficiency < 1. The rate of polymerization was higher at lower  $E_{app}$  values, but polymer dispersity was better at higher (less negative) applied potentials (Table 3, entries 1–3). Lowering the temperature to 55 °C at  $E_{app} = E_{1/2} - 0.06$  V had no significant effect on reaction rate and polymer properties (Table 3, entry 4). Therefore, most of the other experiments were conducted at 55 °C.

**Table 3.** *e*ATRP of methyl methacrylate (MMA) and butyl acrylate in DMF/monomer (50/50, V/V) + 0.1 M  $Et_4NBF_4$  for 5 h<sup>1</sup>.

| Entry           | [EBPA] (mM) | [ $FeCl_3$ ] (mM) | [M]:[I]:[Fe] <sup>2</sup> | $E_{app} - E_{1/2}$ (V) | T (°C) | Q/Qth <sup>3</sup> | Conv. <sup>4</sup> (%) | $10^3 k_{app}$ <sup>5</sup> (min <sup>-1</sup> ) | $M_{n,GPC}$ <sup>6</sup> (kDa) | $M_{n,th}$ <sup>7</sup> (kDa) | $\bar{D}$ <sup>6</sup> |
|-----------------|-------------|-------------------|---------------------------|-------------------------|--------|--------------------|------------------------|--|--------------------------------|-------------------------------|------------------------|
| 1               | 47.0        | 23.5              | 100:1:0.5                 | -0.12                   | 70     | 1.08               | 55.9                   | 27.4   | 6.67                           | 5.84                          | 1.46                   |
| 2               | 47.0        | 23.5              | 100:1:0.5                 | -0.06                   | 70     | 0.85               | 34.4                   | 14.3   | 5.22                           | 3.69                          | 1.33                   |
| 3               | 47.0        | 23.5              | 100:1:0.5                 | 0.0                     | 70     | 0.82               | 26.5                   | 8.5  | 4.02                           | 2.90                          | 1.21                   |
| 4               | 47.0        | 23.5              | 100:1:0.5                 | -0.06                   | 55     | 0.93               | 38.3                   | 16.8   | 6.37                           | 4.33                          | 1.36                   |
| 5               | 47.0        | 11.75             | 100:1:0.25                | -0.06                   | 55     | 1.31               | 43.4                   | 19.7   | 6.47                           | 4.59                          | 1.40                   |
| 6               | 23.5        | 11.75             | 100:0.5:0.25              | -0.06                   | 55     | 1.23               | 32.6                   | 13.5   | 10.24                          | 6.77                          | 1.55                   |
| 7               | 23.5        | 5.88              | 100:0.5:0.126             | -0.06                   | 55     | 1.96               | 38.5                   | 17.8   | 13.34                          | 7.82                          | 1.50                   |
| 8               | 23.5        | 5.88              | 100:0.5:0.126             | 0.0                     | 55     | 1.44               | 23.7                   | 9.92   | 9.13                           | 5.0                           | 1.53                   |
| 9               | 23.5        | 5.88              | 100:0.5:0.126             | 0.0                     | 70     | 1.66               | 48.3                   | 22.7   | 11.66                          | 9.92                          | 1.53                   |
| 10 <sup>8</sup> | 23.5        | 5.88              | 100:0.5:0.126             | -0.06                   | 55     | 1.66               | 40.6                   | 18.2   | 14.75                          | 8.22                          | 1.50                   |
| 11 <sup>9</sup> | 23.5        | 5.88              | 100:0.5:0.126             | -0.06                   | 55     | 0.50               | 0                      | -  | -                              | -                             | -                      |

<sup>1</sup> Other conditions: WE = Pt mesh, CE = graphite rod,  $V = 30$  mL; [MMA] = 4.674 M. <sup>2</sup> [monomer]:[initiator]:[catalyst]. <sup>3</sup> Ratio between passed charge and theoretical value calculated for  $1e^-$  reduction of Fe(III). <sup>4</sup> Monomer conversion. <sup>5</sup> Apparent polymerization rate constant determined as the slope of  $\ln([M]_0/[M])$  vs.  $t$ . <sup>6</sup> Determined by GPC. <sup>7</sup> Theoretical molecular weight. <sup>8</sup> In the presence of a 2-fold excess of TPP with respect to  $FeCl_3$ . <sup>9</sup> In the presence of a 2-fold excess of TPMA with respect to  $FeCl_3$ .

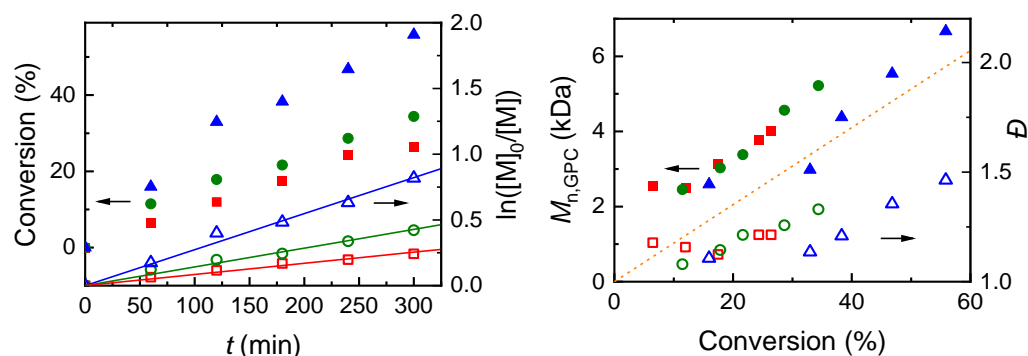


**Figure 9.** *e*ATRP of *m*MMA mediated by  $FeCl_3$  in DMF/*m*MMA (50/50, V/V) + 0.1 M  $Et_4NBF_4$  at 70 °C and  $E_{app} = E_{1/2}$  (squares),  $E_{app} = E_p - 0.06$  V (circles), and  $E_{app} = E_p - 0.12$  V (triangles). The dashed line stands for theoretical  $M_n$ . Other conditions: [MMA]:[EBPA]:[ $FeCl_3$ ] = 100:1:0.5 with [EBPA] = 47.0 mM.

Next, the effect of [EBPA] and [EBPA]/[ $FeCl_3$ ] ratio was tested at  $E_{app} = E_{1/2} - 0.06$  V. Lowering [EBPA] from 47.0 mM to 11.75 mM without changing [EBPA]/[ $FeCl_3$ ] did not appreciably affect polymerization performance; only a slight increase in dispersity was observed (Table 3, entry 5). However, when [EBPA] was also halved, the reaction became slower and polymer dispersity increased to 1.55 (Table 3, entry 6). A further decrease in [EBPA] to 5.88 mM with [EBPA]/[ $FeCl_3$ ] = 23.5 mM slightly decreased the dispersity (Table 3, entry 7). Inter-

estingly, the reaction rate was similar with that of the experiment with  $[\text{FeCl}_3] = 11.75 \text{ mM}$  and  $[\text{EBPA}] = 47.5 \text{ mM}$  (Table 3, entries 5 and 7).

In an attempt to improve polymerization control, the *e*ATRP experiment of entry 7 in Table 3 was repeated at  $E_{\text{app}} = E_{1/2}$ . The dispersity was little affected (slight increase from 1.50 to 1.53) but the reaction rate decreased considerably, with conversion after 5 h dropping from 38.5% to 23.7%. The temperature was then raised to 70 °C to increase the reaction rate. As desired, the conversion increased more than twice while the dispersity remained unchanged (Table 3, entry 9).

Two more experiments were performed to test the role of added ligands. The *e*ATRP of entry 7 (Table 3) was repeated with a two-fold excess of TPP over  $\text{FeCl}_3$  (Table 3, entry 10). Conversion after 5 h increased from 38.5% to 40.6%, while the dispersity remained unchanged. We previously showed that TPP acts as a weak reducing agent rather than a ligand able to form a new complex with  $\text{FeCl}_3$  in DMF. The slight rate enhancement may be attributed to the contribution Fe(II) regeneration via reduction by TPP in the homogeneous phase. The same experiment was again repeated in the presence of TPMA in place of TPP (Table 3, entry 11). No polymerization was observed after 5 h, clearly indicating that  $\text{FeCl}_2(\text{TPMA})$  is not able to activate the initiator.

To sum up, ligand-free  $\text{FeCl}_3$  is a cheap ATRP catalyst able to achieve good polymerization control under appropriate conditions. The efficacy of the catalyst depends on many parameters, including concentrations of catalyst and initiator, type of solvent, temperature and applied potential. Further work systematically addressing the effects of these parameters and their combinations is necessary to define optimal controlled-polymerization conditions.

### 3. Materials and Methods

#### 3.1. Materials

Anhydrous dimethylformamide (DMF) used as solvent in electrochemical investigations was purchased from Sigma-Aldrich, Darmstadt, Germany, (99.8%, anhydrous) and used without further purification.  $\text{FeCl}_3$  (Alfa Aesar, Kandel, Germany, 98%),  $\text{FeCl}_2$  (Alfa Aesar, 98%), tris(2-pyridylmethyl)amine (TPMA, Sigma-Aldrich, 98%),  $\text{CDCl}_3$  (Sigma-Aldrich, 99.8%, anhydrous), LiBr (Alfa Aesar, 99%), basic aluminum oxide ( $\text{Al}_2\text{O}_3$ , Honeywell Riedel-de Haën), DMF (Carlo Erba, Cornaredo, Italy 99.9%, HPLC), ethanol (Carlo Erba, 99.8%), ethyl ether (Sigma-Aldrich, 98%), ethyl  $\alpha$ -bromophenylacetate (EBPA, Alfa Aesar, 97%) and  $\text{H}_2\text{SO}_4$  (Fluka, Buchs, Switzerland, 95%, TraceSELECT) were used as received. Tetraethylammonium tetrafluoroborate ( $\text{Et}_4\text{NBF}_4$ , Alfa Aesar, 99%), used as a background electrolyte, was recrystallized twice from ethanol. Tetraethylammonium chloride (Sigma-Aldrich, 98%), used as a source of  $\text{Cl}^-$  ions in solution, was recrystallized from ethanol/ethyl ether. After recrystallization, both salts were dried in a vacuum oven at 70 °C for 48 h. Methyl methacrylate (Sigma-Aldrich, >99%) was percolated through a column of active basic aluminum oxide to remove polymerization inhibitors. 2-pyridylamino-*N,N*-bis(2-methylene-4,6-dichlorophenol) ( $\text{H}_2\text{L}$ ) and the iron(III) complex  $\text{Fe}^{\text{III}}\text{L}(\text{Cl})$  were prepared following a literature procedure [60] and their purity was checked by NMR (for  $\text{H}_2\text{L}$ ) and elemental analysis (Figure S12, Tables S1 and S2).

#### 3.2. Instrumentation

Electrochemical measurements were carried out in a 5-neck glass cell under an Ar atmosphere; an Autolab PGSTAT 30 or 30N potentiostat/galvanostat (EcoChemie, Utrecht, The Netherlands) run by a PC with GPES or NOVA software (EcoChemie) was used. The working electrode, counter electrode and reference electrode used during voltametric investigations were a 3 mM diameter GC disk (Tokai GC-20), a Pt ring and Ag/AgI/0.1 M *n*-Bu<sub>4</sub>NI in DMF, respectively. Before each experiment, the GC disk was cleaned by polishing with a 0.25  $\mu\text{m}$  diamond paste, followed by ultrasonic rinsing in ethanol for 5 min. The reference electrode was always calibrated with ferrocene (Fc), which was added at the end of each experiment as an internal standard and all potentials are reported versus the fer-



rocenium/ferrocene ( $\text{Fc}^+/\text{Fc}$ ) redox couple. Conversion of these potentials to the saturated calomel electrode scale can be achieved by using  $E^\circ(\text{Fc}^+/\text{Fc}) = 0.476 \text{ V vs. SCE}$  [70].

*e*ATRP experiments were carried out in a two-compartment cell equipped with a Pt mesh (Alfa Aesar, 99.9% metals basis) working electrode, a graphite rod counter electrode and the same reference electrode used in cyclic voltammetry. Before each experiment, the Pt mesh was electrochemically activated in 0.5 M  $\text{H}_2\text{SO}_4$  by cycling the potential from  $-0.7 \text{ V}$  to  $1 \text{ V vs. Hg/Hg}_2\text{SO}_4$  at a scan rate of  $0.2 \text{ V s}^{-1}$  (60 cycles). The counter electrode was separated from the working solution by a glass frit filled with the same electrolyte solution used in the working electrode compartment and a methylcellulose gel saturated with  $\text{Et}_4\text{NBF}_4$ .

Gel permeation chromatography (GPC) was used to determine the number average molecular weight ( $M_n$ ) and dispersity ( $D$ ) of polymers prepared by *e*ATRP. The GPC instrument was Agilent 1260 Infinity, equipped with a refractive index (RI) detector and two PLgel Mixed-D columns (300 mM,  $5 \mu\text{m}$ ) connected in series. The column compartment and RI detector were thermostated at  $70 \text{ }^\circ\text{C}$  and  $50 \text{ }^\circ\text{C}$ , respectively. The eluent was DMF containing 10 mM LiBr, at a flow rate of 1 mL/min. Before injection, the samples were filtered through alumina over a PTFE membrane of 200 nm pore to remove any particulate material and the iron catalyst. The column system was calibrated with 12 linear poly(methyl methacrylate) standards ( $M_n = 540\text{--}2,210,000 \text{ Da}$ ). Monomer conversion was determined by  $^1\text{H-NMR}$  spectroscopy with a 200 MHz Bruker Avance instrument, using  $\text{CDCl}_3$  as a solvent.

UV-Vis spectra were recorded with an Agilent Cary 5000 spectrophotometer by using 10 mM optical path length quartz cuvettes.

### 3.3. *e*ATRP of Methyl Methacrylate

A thermostated 5-neck electrochemical cell, flushed with an inert gas, was loaded with DMF/MMA (50:50, V/V) + 0.1 M  $\text{Et}_4\text{NBF}_4$  and the desired amount of iron catalyst. After recording a CV of the catalyst, the initiator RX was injected, and a CV was recorded. Polymerization was then started by applying the selected applied potential ( $E_{\text{app}}$ ) and samples were withdrawn periodically to measure monomer conversion and  $M_n$  and  $D$  of the polymer.

## 4. Conclusions

In summary, we have shown that  $\text{FeCl}_3$  dissolves in DMF to yield  $\text{FeCl}_4^-$  and  $\text{FeCl}_2^+$ . Reduction of these species gives prevalently  $\text{FeCl}_2$ . A large excess of  $\text{Cl}^-$  is required to convert  $\text{FeCl}_3$  and  $\text{FeCl}_2$  to  $\text{FeCl}_4^-$  and  $\text{FeCl}_4^{2-}$ , respectively. TPMA forms stable complexes with both Fe(III) and Fe(II). 2-Pyridylamino-*N,N*-bis(2-methylene-4,6-dichlorophenolate) (L) also gives a stable iron(III) complex,  $\text{Fe}^{\text{III}}\text{L}(\text{Cl})$ , which provides  $\text{Fe}^{\text{II}}\text{L}(\text{Cl})^-$ , upon one-electron reduction. In contrast, triphenylphosphine does not form a stable complex with  $\text{FeCl}_3$ . It acts as a reducing agent. *e*ATRP of MMA catalyzed by  $\text{Fe}^{\text{III}}\text{L}(\text{Cl})$  was fast and uncontrolled.  $\text{FeCl}_3$  proved to be a much better catalyst than the amine-bis(phenolate) complex.  $\text{FeCl}_3$ -mediated polymerization was well controlled, provided that a large amount of the iron salt was employed. No polymerization was observed when TPMA was used as an additional ligand. It appears that the best catalyst system is the ligand-free iron salt. A weakness of this system is in the deactivation step, characterized by a low rate constant.

**Supplementary Materials:** The following supporting information can be downloaded online: <https://www.mdpi.com/article/10.3390/molecules27196312/s1>, Figure S1: CV of 0.93 mM  $\text{FeCl}_3$  in DMF + 0.1 M  $\text{Et}_4\text{NBF}_4$  + 20 mM  $\text{Et}_4\text{NCl}$ , recorded on a GC electrode at different scan rates at  $T = 25 \text{ }^\circ\text{C}$ ; Figure S2: CV of 1.83 mM  $\text{FeCl}_2$  in DMF + 0.1 M  $\text{Et}_4\text{NBF}_4$  + 20 mM  $\text{Et}_4\text{NCl}$ , recorded on a GC electrode at different scan rates at  $T = 25 \text{ }^\circ\text{C}$ ; Figure S3: fitting of experimental data obtained from CV of  $\text{FeCl}_4^-$  and  $\text{FeCl}_4^{2-}$  on a theoretical working curve (solid line) for the determination of  $k^\circ$  in DMF + 0.1 M  $\text{Et}_4\text{NBF}_4$  at  $T = 25 \text{ }^\circ\text{C}$ ; Figure S4: CV of 1.0 mM  $\text{Fe}^{\text{III}}\text{L}(\text{Cl})$  in DMF + 0.1 M  $\text{Et}_4\text{NBF}_4$  + 30 mM  $\text{Et}_4\text{NCl}$ , recorded on a GC electrode at different scan rates at  $T = 25 \text{ }^\circ\text{C}$ ; Figure S5: fitting of experimental data obtained from CV of  $\text{Fe}^{\text{III}}\text{L}(\text{Cl})$  on a theoretical working curve



(solid line) for the determination of  $k^\circ$  in DMF + 0.1 M Et<sub>4</sub>NBF<sub>4</sub> at  $T = 25^\circ\text{C}$ ; Figure S6: UV-vis spectra of 0.1 mM FeCl<sub>3</sub>, 0.2 mM TPP and a mixture of 0.1 mM FeCl<sub>3</sub> + 0.2 mM TPP, in DMF; Figure S7: CV of 1.08 mM FeCl<sub>2</sub> in DMF + 0.1 M Et<sub>4</sub>NBF<sub>4</sub>, recorded on a GC electrode in the absence and presence of triphenylphosphine (TPP) at  $v = 0.2\text{ V/s}$  and  $T = 25^\circ\text{C}$ ; Figure S8: CV of 1.1 mM FeCl<sub>3</sub> in DMF + 0.1 M Et<sub>4</sub>NBF<sub>4</sub> recorded on a GC electrode at  $v = 0.2\text{ V/s}$  and  $T = 25^\circ\text{C}$ , before and after addition of TPMA and Et<sub>4</sub>NCl; Figure S9: CV of 5 mM Fe<sup>III</sup>L(Cl) in DMF/MMA (50/50, V/V) + 0.1 M Et<sub>4</sub>NBF<sub>4</sub> recorded on a GC electrode at  $v = 0.2\text{ V/s}$  and  $T = 50^\circ\text{C}$ , in the absence (black line) and presence of 15 mM ECPA (blue line) or 15 mM EBPA (red line); Figure S10: GPC traces of PMMA samples taken at different monomer conversions during eATRP of mMA mediated by Fe<sup>III</sup>L(Cl) in DMF/MMA (50/50, V/V) + 0.1 M Et<sub>4</sub>NBF<sub>4</sub> with EBPA as initiator performed at  $50^\circ\text{C}$  and  $E_{\text{app}} = E_p + 0.06\text{ V}$ ; Figure S11: CV of 11.75 mM FeCl<sub>3</sub> in DMF/MMA (50/50, V/V) + 0.1 M Et<sub>4</sub>NBF<sub>4</sub> recorded on a GC electrode at  $v = 0.2\text{ V/s}$  and  $T = 55^\circ\text{C}$ , in the absence (black line) and presence of 47 mM EBPA (red line); Figure S12: <sup>1</sup>H NMR spectrum (300 MHz, CDCl<sub>3</sub>) of 2-pyridylamino-*N,N*-bis(2-methylene-4,6-dichlorophenol); Table S1: <sup>1</sup>H NMR spectral data of 2-pyridylamino-*N,N*-bis(2-methylene-4,6-dichlorophenol); Table S2: Elemental analysis of chloro(2-pyridylamino-*N,N*-bis(2-methylene-4,6-dichlorophenolate))iron(III). Ref. [60] is cited in Supplementary Materials.

**Author Contributions:** Conceptualization, A.A.I. and M.F.; methodology, A.A.I. and M.F.; investigation, G.G. and S.P.; resources, C.D. and A.A.I.; validation, G.G. and N.B.; data curation, all authors; writing—original draft preparation, A.A.I.; writing—review and editing, all authors; supervision, A.A.I., M.F., C.T.; All authors have read and agreed to the published version of the manuscript.

**Funding:** This research received no external funding.

**Institutional Review Board Statement:** Not applicable.

**Informed Consent Statement:** Not applicable.

**Data Availability Statement:** Data obtained in this study are available in the article and Supporting Materials.

**Acknowledgments:** We gratefully acknowledge the University of Padova for financial support (Fondi DOR).

**Conflicts of Interest:** The authors declare no conflict of interest.

**Sample Availability:** Samples of the compounds are not available from the authors.

## References

1. Corrigan, N.; Jung, K.; Moad, G.; Hawker, C.J.; Matyjaszewski, K.; Boyer, C. Reversible-Deactivation Radical Polymerization (Controlled/Living Radical Polymerization): From Discovery to Materials Design and Applications. *Progress Polym. Sci.* **2020**, *111*, 101311. [[CrossRef](#)]
2. Matyjaszewski, K. Atom Transfer Radical Polymerization (ATRP): Current Status and Future Perspectives. *Macromolecules* **2012**, *45*, 4015–4039. [[CrossRef](#)]
3. Ribelli, T.G.; Lorandi, F.; Fantin, M.; Matyjaszewski, K. Atom Transfer Radical Polymerization: Billion Times More Active Catalysts and New Initiation Systems. *Macromol. Rapid Commun.* **2019**, *40*, 1800616. [[CrossRef](#)]
4. Lorandi, F.; Fantin, M.; Matyjaszewski, K. Atom Transfer Radical Polymerization: A Mechanistic Perspective. *J. Am. Chem. Soc.* **2022**, *144*, 15413–15430. [[CrossRef](#)]
5. Moad, G.; Rizzardo, E.; Thang, S.H. Living Radical Polymerization by the RAFT Process. *Aust. J. Chem.* **2005**, *58*, 379. [[CrossRef](#)]
6. Perrier, S. 50th Anniversary Perspective: RAFT Polymerization—A User Guide. *Macromolecules* **2017**, *50*, 7433–7447. [[CrossRef](#)]
7. Nicolas, J.; Guillaneuf, Y.; Lefay, C.; Bertin, D.; Gimes, D.; Charleux, B. Nitroxide-Mediated Polymerization. *Progress Polym. Sci.* **2013**, *38*, 63–235. [[CrossRef](#)]
8. Audran, G.; Bagryanskaya, E.G.; Marque, S.R.A.; Postnikov, P. New Variants of Nitroxide Mediated Polymerization. *Polymers* **2020**, *12*, 1481. [[CrossRef](#)]
9. Ching, Y.L.; Coote, M.L.; Gennaro, A.; Matyjaszewski, K. Ab Initio Evaluation of the Thermodynamic and Electrochemical Properties of Alkyl Halides and Radicals and Their Mechanistic Implications for Atom Transfer Radical Polymerization. *J. Am. Chem. Soc.* **2008**, *130*, 12762–12774. [[CrossRef](#)]
10. Isse, A.A.; Gennaro, A.; Lin, C.Y.; Hodgson, J.L.; Coote, M.L.; Guliashvili, T. Mechanism of Carbon-Halogen Bond Reductive Cleavage in Activated Alkyl Halide Initiators Relevant to Living Radical Polymerization: Theoretical and Experimental Study. *J. Am. Chem. Soc.* **2011**, *133*, 6254–6264. [[CrossRef](#)]
11. Isse, A.A.; Bortolamei, N.; de Paoli, P.; Gennaro, A. On the Mechanism of Activation of Copper-Catalyzed Atom Transfer Radical Polymerization. *Electrochim. Acta* **2013**, *110*, 655–662. [[CrossRef](#)]

12. Pan, X.; Fantin, M.; Yuan, F.; Matyjaszewski, K. Externally Controlled Atom Transfer Radical Polymerization. *Chem. Soc. Rev.* **2018**, *47*, 5457–5490. [[CrossRef](#)]
13. Min, K.; Gao, H.; Matyjaszewski, K. Use of Ascorbic Acid as Reducing Agent for Synthesis of Well-Defined Polymers by ARGET ATRP. *Macromolecules* **2007**, *40*, 1789–1791. [[CrossRef](#)]
14. Simakova, A.; Averick, S.E.; Konkolewicz, D.; Matyjaszewski, K. Aqueous ARGET ATRP. *Macromolecules* **2012**, *45*, 6371–6379. [[CrossRef](#)]
15. Mendonça, P.V.; Ribeiro, J.P.M.; Abreu, C.M.R.; Guliasvili, T.; Serra, A.C.; Coelho, J.F.J. Thiourea Dioxide As a Green and Affordable Reducing Agent for the ARGET ATRP of Acrylates, Methacrylates, Styrene, Acrylonitrile, and Vinyl Chloride. *ACS Macro Lett.* **2019**, *8*, 315–319. [[CrossRef](#)]
16. Percec, V.; Guliasvili, T.; Ladislav, J.S.; Wistrand, A.; Stjern Dahl, A.; Sienkowska, M.J.; Monteiro, M.J.; Sahoo, S. Ultrafast Synthesis of Ultrahigh Molar Mass Polymers by Metal-Catalyzed Living Radical Polymerization of Acrylates, Methacrylates, and Vinyl Chloride Mediated by SET at 25 °C. *J. Am. Chem. Soc.* **2006**, *128*, 14156–14165. [[CrossRef](#)]
17. Zhang, Y.Z.; Wang, Y.; Matyjaszewski, K. ATRP of Methyl Acrylate with Metallic Zinc, Magnesium, and Iron as Reducing Agents and Supplemental Activators. *Macromolecules* **2011**, *44*, 683–685. [[CrossRef](#)]
18. Lorandi, F.; Fantin, M.; Isse, A.A.; Gennaro, A. RDRP in the Presence of Cu0: The Fate of Cu(I) Proves the Inconsistency of SET-LRP Mechanism. *Polymer* **2015**, *72*, 238–245. [[CrossRef](#)]
19. Chmielarz, P.; Fantin, M.; Park, S.; Isse, A.A.; Gennaro, A.; Magenau, A.J.D.; Sobkowiak, A.; Matyjaszewski, K. Electrochemically Mediated Atom Transfer Radical Polymerization (EATRP). *Progress Polym. Sci.* **2017**, *69*, 47–78. [[CrossRef](#)]
20. Lorandi, F.; Fantin, M.; Isse, A.A.; Gennaro, A. Electrochemical Triggering and Control of Atom Transfer Radical Polymerization. *Curr. Opin. Electrochem.* **2018**, *8*, 1–7. [[CrossRef](#)]
21. Tasdelen, M.A.; Uygun, M.; Yagci, Y. Photoinduced Controlled Radical Polymerization. *Macromol. Rapid Commun.* **2011**, *32*, 58–62. [[CrossRef](#)]
22. Konkolewicz, D.; Schröder, K.; Buback, J.; Bernhard, S.; Matyjaszewski, K. Visible Light and Sunlight Photoinduced ATRP with Ppm of Cu Catalyst. *ACS Macro Lett.* **2012**, *1*, 1219–1223. [[CrossRef](#)]
23. Anastasaki, A.; Nikolaou, V.; Zhang, Q.; Burns, J.; Samanta, S.R.; Waldron, C.; Haddleton, A.J.; McHale, R.; Fox, D.; Percec, V.; et al. Copper(II)/Tertiary Amine Synergy in Photoinduced Living Radical Polymerization: Accelerated Synthesis of  $\omega$ -Functional and  $\alpha,\omega$ -Heterofunctional Poly(Acrylates). *J. Am. Chem. Soc.* **2014**, *136*, 1141–1149. [[CrossRef](#)]
24. Mohapatra, H.; Kleiman, M.; Esser-Kahn, A.P. Mechanically Controlled Radical Polymerization Initiated by Ultrasound. *Nat. Chem.* **2017**, *9*, 135–139. [[CrossRef](#)]
25. Zaborniak, I.; Chmielarz, P. Ultrasound-Mediated Atom Transfer Radical Polymerization (ATRP). *Materials* **2019**, *12*, 3600. [[CrossRef](#)]
26. Soly, S.; Mistry, B.; Murthy, C.N. Photo-Mediated Metal-Free Atom Transfer Radical Polymerization: Recent Advances in Organocatalysts and Perfection towards Polymer Synthesis. *Polym. Int.* **2022**, *71*, 159–168. [[CrossRef](#)]
27. Pan, X.; Fang, C.; Fantin, M.; Malhotra, N.; So, W.Y.; Peteanu, L.A.; Isse, A.A.; Gennaro, A.; Liu, P.; Matyjaszewski, K. Mechanism of Photoinduced Metal-Free Atom Transfer Radical Polymerization: Experimental and Computational Studies. *J. Am. Chem. Soc.* **2016**, *138*, 2411–2425. [[CrossRef](#)]
28. Di Lena, F.; Matyjaszewski, K. Transition Metal Catalysts for Controlled Radical Polymerization. *Progress Polym. Sci.* **2010**, *35*, 959–1021. [[CrossRef](#)]
29. Jain, T.K.; Reddy, M.K.; Morales, M.A.; Leslie-Pelecky, D.L.; Labhasetwar, V. Biodistribution, Clearance, and Biocompatibility of Iron Oxide Magnetic Nanoparticles in Rats. *Mol. Pharm.* **2008**, *5*, 316–327. [[CrossRef](#)]
30. Oriňaková, R.; Oriňak, A.; Giretová, M.; Medvecký, L.; Kupková, M.; Hrubovčíáková, M.; Maskal'ová, I.; MacKo, J.; Kal'Avský, F. A Study of Cytocompatibility and Degradation of Iron-Based Biodegradable Materials. *J. Biomater. Appl.* **2016**, *30*, 1060–1070. [[CrossRef](#)]
31. Dadashi-Silab, S.; Matyjaszewski, K. Iron Catalysts in Atom Transfer Radical Polymerization. *Molecules* **2020**, *25*, 1648. [[CrossRef](#)] [[PubMed](#)]
32. Xue, Z.; He, D.; Xie, X. Iron-Catalyzed Atom Transfer Radical Polymerization. *Polym. Chem.* **2015**, *6*, 1660–1687. [[CrossRef](#)]
33. Uchiike, C.; Terashima, T.; Ouchi, M.; Ando, T.; Kamigaito, M.; Sawamoto, M. Evolution of Iron Catalysts for Effective Living Radical Polymerization: Design of Phosphine/Halogen Ligands in FeX<sub>2</sub>(PR<sub>3</sub>)<sub>2</sub>. *Macromolecules* **2007**, *40*, 8658–8662. [[CrossRef](#)]
34. Nishizawa, K.; Ouchi, M.; Sawamoto, M. Phosphine–Ligand Decoration toward Active and Robust Iron Catalysts in LRP. *Macromolecules* **2013**, *46*, 3342–3349. [[CrossRef](#)]
35. Wang, J.; Han, J.; Xie, X.; Xue, Z.; Fliedel, C.; Poli, R. FeBr<sub>2</sub>-Catalyzed Bulk ATRP Promoted by Simple Inorganic Salts. *Macromolecules* **2019**, *52*, 5366–5376. [[CrossRef](#)]
36. Mukumoto, K.; Wang, Y.; Matyjaszewski, K. Iron-Based ICAR ATRP of Styrene with Ppm Amounts of FeIII Br<sub>3</sub> and 1,1'-Azobis(Cyclohexanecarbonitrile). *ACS Macro Lett.* **2012**, *1*, 599–602. [[CrossRef](#)]
37. Allan, L.E.N.; MacDonald, J.P.; Reckling, A.M.; Kozak, C.M.; Shaver, M.P. Controlled Radical Polymerization Mediated by Amine-Bis(Phenolate) Iron(III) Complexes. *Macromol. Rapid Commun.* **2012**, *33*, 414–418. [[CrossRef](#)]
38. Schroeder, H.; Buback, M.; Matyjaszewski, K. Pressure Dependence of Iron-Mediated Methyl Methacrylate ATRP in Different Solvent Environments. *Macromol. Chem. Phys.* **2014**, *215*, 44–53. [[CrossRef](#)]
39. Dadashi-Silab, S.; Kim, K.; Lorandi, F.; Schild, D.J.; Fantin, M.; Matyjaszewski, K. Effect of Halogen and Solvent on Iron-Catalyzed Atom Transfer Radical Polymerization. *Polym. Chem.* **2022**, *13*, 1059–1066. [[CrossRef](#)]

40. Simakova, A.; Mackenzie, M.; Averick, S.E.; Park, S.; Matyjaszewski, K. Bioinspired Iron-Based Catalyst for Atom Transfer Radical Polymerization. *Angew. Chem. Int. Ed.* **2013**, *52*, 12148–12151. [[CrossRef](#)]
41. Yang, D.; He, D.; Liao, Y.; Xue, Z.; Zhou, X.; Xie, X. Iron-Mediated AGET ATRP of Methyl Methacrylate in the Presence of Polar Solvents as Ligands. *J. Polym. Sci. A Polym. Chem.* **2014**, *52*, 1020–1027. [[CrossRef](#)]
42. Dadashi-Silab, S.; Pan, X.; Matyjaszewski, K. Photoinduced Iron-Catalyzed Atom Transfer Radical Polymerization with Ppm Levels of Iron Catalyst under Blue Light Irradiation. *Macromolecules* **2017**, *50*, 7967–7977. [[CrossRef](#)]
43. Rolland, M.; Truong, N.P.; Whitfield, R.; Anastasaki, A. Tailoring Polymer Dispersity in Photoinduced Iron-Catalyzed ATRP. *ACS Macro Lett.* **2020**, *9*, 459–463. [[CrossRef](#)] [[PubMed](#)]
44. Guo, J.K.; Zhou, Y.N.; Luo, Z.H. Kinetic Insights into the Iron-Based Electrochemically Mediated Atom Transfer Radical Polymerization of Methyl Methacrylate. *Macromolecules* **2016**, *49*, 4038–4046. [[CrossRef](#)]
45. Guo, J.K.; Zhou, Y.N.; Luo, Z.H. Iron-Based Electrochemically Mediated Atom Transfer Radical Polymerization with Tunable Catalytic Activity. *AIChE J.* **2018**, *64*, 961–969. [[CrossRef](#)]
46. Wang, J.; Tian, M.; Li, S.; Wang, R.; Du, F.; Xue, Z. Ligand-Free Iron-Based Electrochemically Mediated Atom Transfer Radical Polymerization of Methyl Methacrylate. *Polym. Chem.* **2018**, *9*, 4386–4394. [[CrossRef](#)]
47. Divandari, M.; Pollard, J.; Dehghani, E.; Bruns, N.; Benetti, E.M. Controlling Enzymatic Polymerization from Surfaces with Switchable Bioaffinity. *Biomacromolecules* **2017**, *18*, 4261–4270. [[CrossRef](#)]
48. Sigg, S.J.; Seidi, F.; Renggli, K.; Silva, T.B.; Kali, G.; Bruns, N. Horseradish Peroxidase as a Catalyst for Atom Transfer Radical Polymerization. *Macromol. Rapid Commun.* **2011**, *32*, 1710–1715. [[CrossRef](#)]
49. Silva, T.B.; Spulber, M.; Kocik, M.K.; Seidi, F.; Charan, H.; Rother, M.; Sigg, S.J.; Renggli, K.; Kali, G.; Bruns, N. Hemoglobin and Red Blood Cells Catalyze Atom Transfer Radical Polymerization. *Biomacromolecules* **2013**, *14*, 2703–2712. [[CrossRef](#)]
50. Rifaie-Graham, O.; Pollard, J.; Raccio, S.; Balog, S.; Rusch, S.; Hernández-Castañeda, M.A.; Mantel, P.-Y.; Beck, H.-P.; Bruns, N. Hemozoin-Catalyzed Precipitation Polymerization as an Assay for Malaria Diagnosis. *Nat. Commun.* **2019**, *10*, 1369. [[CrossRef](#)]
51. Pollard, J.; Rifaie-Graham, O.; Raccio, S.; Davey, A.; Balog, S.; Bruns, N. Biocatalytically Initiated Precipitation Atom Transfer Radical Polymerization (ATRP) as a Quantitative Method for Hemoglobin Detection in Biological Fluids. *Anal. Chem.* **2020**, *92*, 1162–1170. [[CrossRef](#)] [[PubMed](#)]
52. Raccio, S.; Pollard, J.; Djuhadi, A.; Balog, S.; Pellizzoni, M.M.; Rodriguez, K.J.; Rifaie-Graham, O.; Bruns, N. Rapid Quantification of the Malaria Biomarker Hemozoin by Improved Biocatalytically Initiated Precipitation Atom Transfer Radical Polymerizations. *Analyst* **2020**, *145*, 7741–7751. [[CrossRef](#)] [[PubMed](#)]
53. De Bon, F.; Fantin, M.; Isse, A.A.; Gennaro, A. Electrochemically Mediated ATRP in Ionic Liquids: Controlled Polymerization of Methyl Acrylate in [BMIm][OTf]. *Polym. Chem.* **2018**, *9*, 646–655. [[CrossRef](#)]
54. Fantin, M.; Isse, A.A.; Venzo, A.; Gennaro, A.; Matyjaszewski, K. Atom Transfer Radical Polymerization of Methacrylic Acid: A Won Challenge. *J. Am. Chem. Soc.* **2016**, *138*, 7216–7219. [[CrossRef](#)] [[PubMed](#)]
55. Bonometti, V.; Labbé, E.; Buriez, O.; Mussini, P.; Amatore, C. Exploring the First Steps of an Electrochemically-Triggered Controlled Polymerization Sequence: Activation of Alkyl- and Benzyl Halide Initiators by an Electrogenerated FeII Salen Complex. *J. Electroanal. Chem.* **2009**, *633*, 99–105. [[CrossRef](#)]
56. Dass, N.N.; George, M.H. IRON(II)-chloro complexes in n,n-dimethylformamidyl styrene systems. *Polym. Lett.* **1967**, *5*, 1119–1124. [[CrossRef](#)]
57. Kim, Y.J.; Park, C.R. Analysis of Problematic Complexing Behavior of Ferric Chloride with N,N-Dimethylformamide Using Combined Techniques of FT-IR, XPS, and TGA/DTG. *Inorg. Chem.* **2002**, *41*, 6211–6216. [[CrossRef](#)]
58. Bard, A.J.; Faulkner, L.R. *Electrochemical Methods: Fundamentals and Applications*, 2nd ed.; John Wiley & Sons: New York, NY, USA, 2011; ISBN 0-471-04372-9.
59. Nicholson, R.S. Theory and Application of Cyclic Voltammetry for Measurement of Electrode Reaction Kinetics. *Anal. Chem.* **1965**, *37*, 1351–1355. [[CrossRef](#)]
60. Reckling, A.M.; Martin, D.; Dawe, L.N.; Decken, A.; Kozak, C.M. Structure and C–C Cross-Coupling Reactivity of Iron(III) Complexes of Halogenated Amine-Bis(Phenolate) Ligands. *J. Organom. Chem.* **2011**, *696*, 787–794. [[CrossRef](#)]
61. David Walker, J.; Poli, R. *FeCl<sub>3</sub>-Phosphine Adducts with Trigonal-Bipyramidal Geometry. Influence of the Phosphine on the Spin State*; HAL Open Science: Lyon, France, 1989; Volume 28.
62. Wang, Y.; Kwak, Y.; Matyjaszewski, K. Enhanced Activity of ATRP Fe Catalysts with Phosphines Containing Electron Donating Groups. *Macromolecules* **2012**, *45*, 5911–5915. [[CrossRef](#)]
63. Schroeder, H.; Matyjaszewski, K.; Buback, M. Kinetics of Fe-Mediated ATRP with Triarylphosphines. *Macromolecules* **2015**, *48*, 4431–4437. [[CrossRef](#)]
64. Kojima, T.; Leising, R.A.; Yan, S.; Que, L. Alkane Functionalization at Nonheme Iron Centers. Stoichiometric Transfer of Metal-Bound Ligands to Alkane. *J. Am. Chem. Soc.* **1993**, *115*, 11328–11335. [[CrossRef](#)]
65. Mandon, D.; Machkour, A.; Goetz, S.; Welter, R. Trigonal Bipyramidal Geometry and Tridentate Coordination Mode of the Tripod in FeCl<sub>2</sub> Complexes with Tris(2-Pyridylmethyl)Amine Derivatives Bis- $\alpha$ -Substituted with Bulky Groups. Structures and Spectroscopic Comparative Studies. *Inorg. Chem.* **2002**, *41*, 5364–5372. [[CrossRef](#)] [[PubMed](#)]
66. George, J.; Sastry, N.V. Densities, Excess Molar Volumes at  $T = (298.15 \text{ to } 313.15) \text{ K}$ , Speeds of Sound, Excess Isentropic Compressibilities, Relative Permittivities, and Deviations in Molar Polarizations at  $T = (298.15 \text{ and } 308.15) \text{ K}$  for Methyl Methacrylate + 2-Butoxyethanol or Dibutyl Ether + Benzene, Toluene, or *p*-Xylene. *J. Chem. Eng. Data* **2004**, *49*, 1116–1126. [[CrossRef](#)]

67. Wohlfarth, C. Permittivity (Dielectric Constant) of Liquids. In *CRC Handbook of Chemistry and Physics*; Lide, D.R., Ed.; Taylor and Francis: Boca Raton, FL, USA, 2007.
68. Allan, L.E.N.; Macdonald, J.P.; Nichol, G.S.; Shaver, M.P. Single Component Iron Catalysts for Atom Transfer and Organometallic Mediated Radical Polymerizations: Mechanistic Studies and Reaction Scope. *Macromolecules* **2014**, *47*, 1249–1257. [[CrossRef](#)]
69. Schroeder, H.; Buback, M. SP-PLP-EPR Measurement of Iron-Mediated ATRP Deactivation Rate. *Macromolecules* **2015**, *48*, 6108–6113. [[CrossRef](#)]
70. Falciola, L.; Gennaro, A.; Isse, A.A.; Mussini, P.R.; Rossi, M. The Solvent Effect in the Electrocatalytic Reduction of Organic Bromides on Silver. *J. Electroanal. Chem.* **2006**, *593*, 47–56. [[CrossRef](#)]